Z. angew. Math. Phys. 57 (2006) 875–903
0044-2275/06/050875-29
DOI 10.1007/s00033-006-0067-4

Zeitschrift für angewandte Mathematik und Physik ZAMP

Micro/nano sliding plate problem with Navier boundary condition

Miccal T. Matthews* and James M. Hill

Abstract. For Newtonian flow through micro or nano sized channels, the no-slip boundary condition does not apply and must be replaced by a condition which more properly reflects surface roughness. Here we adopt the so-called Navier boundary condition for the sliding plate problem, which is one of the fundamental problems of fluid mechanics. When the no-slip boundary condition is used in the study of the motion of a viscous Newtonian fluid near the intersection of fixed and moving rigid plane boundaries, singular pressure and stress profiles are obtained, leading to a non-integrable force on each boundary. Here we examine the effects of replacing the no-slip boundary condition by a boundary condition which attempts to account for boundary slip due to the tangential shear at the boundary. The Navier boundary condition, possesses a single parameter to account for the slip, the slip length ℓ, and two solutions are obtained; one integral transform solution and a similarity solution which is valid away from the corner. For the former the tangential stress on each boundary is obtained as a solution of a set of coupled integral equations. The particular case solved is right-angled corner flow and equal slip lengths on each boundary. It is found that when the slip length is non-zero the force on each boundary is finite. It is also found that for a sufficiently large distance from the corner the tangential stress on each boundary is equal to that of the classical solution. The similarity solution involves two restrictions, either a right-angled corner flow or a dependence on the two slip lengths for each boundary. When the tangential stress on each boundary is calculated from the similarity solution, it is found that the similarity solution makes no additional contribution to the tangential stress of that of the classical solution, thus in agreement with the findings of the integral transform solution. Values of the radial component of velocity along the line $\theta = \pi/4$ for increasing distance from the corner for the similarity and integral transform solutions are compared, confirming their agreement for sufficiently large distances from the corner.

Keywords. Sliding plate problem, Navier boundary condition, nanofluidics.

1. Introduction

For many problems at the micro or nano scale, the boundary surface roughness may be significant in comparison to the dimensions of the flow. In this event the usual no-slip boundary condition of fluid mechanics does not apply, and must be replaced by a condition which reflects boundary slip as a consequence of the tangential shear

*Corresponding author.

at the boundary. The simplest linear boundary condition to accommodate this is the so-called Navier boundary condition, first proposed by Navier in 1823 [23] and later independently by Maxwell in 1879 [16]. This condition suggests that the boundary slip is directly proportional to the tangential shear at the boundary, and the constant of proportionality is referred to as the slip length. The slip length may be regarded as the distance at which the velocity of the fluid is equal to that of the boundary if it were linearly extrapolated beyond the boundary (Lauga et al. [14]). In this paper we consider the problem of viscous flow between fixed and moving rigid plane boundaries, assuming a Navier boundary condition with generally distinct constant slip lengths on each boundary.

When an incompressible viscous fluid is contained in a corner between two boundaries and one moves at a constant velocity parallel to itself, the flow generated is dominated by viscous forces sufficiently close to the corner (Hancock et al. [6]). This problem is generally known as the sliding plate problem, and was first considered by Taylor [35] and Goodier [5]. In the region near the corner where viscous forces are dominant, the stream function ψ satisfies the biharmonic equation $\nabla^4\psi = 0$, and for no-slip at the boundaries a solution may be found which satisfies all the required boundary conditions. Contour plots of the streamline patterns near the corner provide the well-known picture of declined streamlines (Meleshko [19]).

Expressions for the pressure and stress for the classical solution vary as r^{-1}, that is there is a logarithmic singularity when the force on each boundary is calculated. As pointed out by Shikhmurzaev [33, 32] the presence of this singularity is physically unacceptable. There have been many suggestions for this singularity; for example Koplik and Banavar [11] suggest that the fluid is non-Newtonian in the corner. However, the breakdown in the analysis may be seen to be a direct consequence of the no-slip boundary condition applied at the boundaries. The above-mentioned analysis employees the no-slip boundary condition at each boundary, that is zero relative velocity is assumed between the fluid and boundary, which is a fundamental notion in classical fluid mechanics (see for example Batchelor [2]). Since one boundary is stationary while the other moves with a constant velocity, the no-slip boundary condition implies that at the corner where the two boundaries meet, there is a discontinuity in the fluid velocity. This requires an infinite acceleration of the fluid, which violates the slow flow assumption.

There are at least two ways to attempt to remove this singularity. The first is to assume that the velocity of the fluid at each boundary is not equal to the constant velocity of the boundary, but instead has some functional dependence. This has been assumed for the sliding plate problem in the analysis of Krasnopolskaya [12] and also for the moving contact line problem by Dussan [3]. The moving contact line problem is where one fluid displaces another fluid along a boundary, and similarity solutions obtained by Huh and Scriven [10] show a non-integrable stress and pressure singularity, similar to that of the sliding plate problem. The method of replacing the constant velocity boundary condition with a functional

dependence has proven successful in removing these singularities, however these mathematical devices do not correspond to physical experimental conditions.

The second method involves replacing the no-slip boundary condition by one depending on the tangential shear, such as the Navier boundary condition. Although the amount of slip depends on molecular details, Hocking [8] and Lamb [13] have suggested that the overall effect on the flow on a macroscopic scale can be obtained by postulating a dynamic boundary condition in which the relative velocity at the boundary is proportional to the tangential viscous stress there; that is the net tangential force per unit area exerted on the solid due to the hydrodynamic motion of the surrounding fluid (Qian et al. [25]). The constant of proportionality which expresses the ratio of the relative velocity to the tangential viscous stress is termed the slip length, denoted by ℓ. As demonstrated by Qian and Wang [24], for a Newtonian fluid, the tangential viscous stress is proportional to the shear rate; consequently, the amount of slip is proportional to the shear rate. As pointed out by Hocking [9] such an analysis does not provide a complete analysis of the flow, but overall features such as the total stress on a boundary may be inferred. A complete analysis is only possible for relatively simple flows, such as that around a nanosphere or nanocylinder (Matthews and Hill [15]). For micro-cylinders the present authors show conclusively that the Navier boundary condition gives rise to results which are in excellent agreement with longstanding experimental results which were poorly represented by the then existing theory. In two papers, Hocking [8, 9] details the microscopic origin of the Navier boundary condition as a result of surface irregularities and studied the moving contact line problem with a Navier boundary condition. The tangential stress on each boundary is obtained from a set of coupled integral equations, and these results demonstrate that the force on each boundary is finite for a nonzero slip length.

The validity of the Navier boundary condition has been shown Qian and Wang [24] for the sliding plate problem through molecular dynamic and continuum hydrodynamic simulation for a Newtonian fluid. The (constant) slip length is determined from molecular dynamics simulations, usually ranging from one to a few nanometers, and when used as an input for the continuum hydrodynamic simulation it has been shown by Qian et al. [26, 27] that molecular dynamics results can be successfully reproduced.

The Navier boundary condition assumes that the degree of slip is independent of the shear rate, that is ℓ is constant, although recent molecular dynamic simulations by Thompson and Troian [36] have indicated that ℓ is a nonlinear function of the shear rate over a large range of shear rates. At low shear rates, the Navier boundary condition is valid, that is ℓ is constant, but at high shear rates the Navier boundary condition breaks down as ℓ increases rapidly with the shear rate. Thus, the Navier boundary condition is a low-shear-rate limit of a more generalized universal relationship which is significantly nonlinear and divergent at a (high) critical shear rate. Modelling flows based on a functional dependence of the slip length on the tangential viscous stress would be inherently difficult, and possibly

intractable analytically except for specific problems with simple flow geometries. Since in the problem studied here the flow is assumed to be slow, these matters are of little consequence.

In this paper the linear Navier boundary condition with a constant but general slip length is applied to the steady viscous flow of a Newtonian fluid between a fixed and moving boundary, at length scales where the slip length is relevant. In the following section, the equations describing the Navier boundary condition are presented. In section 3 an overview of the solution corresponding to a no-slip boundary condition at each boundary is presented. In sections 4 and 5 we develop an integral transform solution assuming the Navier boundary condition applies on each boundary, while in section 6 we determine a similarity solution which is valid away from the corner. In section 7 some numerical results and general features of the solutions obtained are discussed, as well as concluding remarks. In appendix A we present a derivation of an approximate analytical expression for the governing set of integral equations, while in appendix B we present the details for the derivation of the radial component of velocity along the line $\theta = \pi/4$ for the integral transform solution. Given that a large number of transformations are necessary a nomenclature for some of the basic variables are presented in appendix C. Finally, we comment that in principle we might adopt for the integral transform solution either a two-sided Laplace transform or a Mellin transform; the two are theoretically equivalent. However, in practice depending on the task at hand, one is often more convenient than the other. Accordingly, the two-sided Laplace transform is used in the main paper, while the Mellin transform is exploited in appendix B.

2. Navier boundary condition

The standard no-slip boundary condition at the boundary is replaced by the Navier boundary condition, where the slip velocity is assumed to be proportional to the tangential viscous stress and the degree of slip is measured by a constant slip length. For an incompressible Newtonian fluid the viscous portion of the stress tensor or the extra stress is given by $\mathbf{S} = 2\mu\mathbf{D}$, where μ is the viscosity and the rate of deformation tensor is

$$\mathbf{D} = \frac{1}{2}\left[\nabla\mathbf{v} + (\nabla\mathbf{v})^T\right], \tag{2.1}$$

i.e. $\mathbf{S} \propto \mathbf{D}$. For the sliding plate problem in cylindrical coordinates, the Navier boundary condition at the corresponding boundary implies $v_\theta \propto D_{r\theta}$, where from Slattery [34]

$$D_{r\theta} = \frac{1}{2}\left[\frac{\partial v_\theta}{\partial r} - \frac{1}{r}\left(v_\theta - \frac{\partial v_r}{\partial \theta}\right)\right]. \tag{2.2}$$

At each boundary the normal velocity is $v_\theta = 0$ and therefore $\partial v_\theta/\partial r = 0$ (see Happel and Brenner [7]), so that the Navier boundary condition at the boundary

is given by

$$v_r = \frac{\ell}{r}\frac{\partial v_r}{\partial \theta}, \tag{2.3}$$

where ℓ is the slip length.

3. Basic equations and no-slip solution

Consider the flow of a viscous fluid in a corner between two rigid solid plates, one of which slides with a steady velocity U relative to the other at a constant inclination angle θ_0. The problem can be considered steady by choosing an origin of coordinates fixed and moving with the intersection of the two plates. A cylindrical coordinate system (r, θ, z) will be used such that

$$v_r = v_x \cos\theta + v_y \sin\theta, \;\; v_\theta = -v_x \sin\theta + v_y \cos\theta. \tag{3.1}$$

The relevant boundary conditions are given by

$$\begin{gathered} v_r = -U, \;\; v_\theta = 0, \;\; \theta = 0, \\ v_r = 0, \;\; v_\theta = 0, \;\; \theta = \theta_0. \end{gathered} \tag{3.2}$$

It is assumed that

$$v_r = v_r(r, \theta), \;\; v_\theta = v_\theta(r, \theta), \;\; v_z = 0, \tag{3.3}$$

so that a stream function $\psi(r, \theta)$ defined by

$$v_r = \frac{1}{r}\frac{\partial \psi}{\partial \theta}, \;\; v_\theta = -\frac{\partial \psi}{\partial r}, \tag{3.4}$$

may be introduced such that the differential mass conservation equation is automatically satisfied. In terms of this stream function the boundary conditions may be written

$$\begin{gathered} \frac{1}{r}\frac{\partial \psi}{\partial \theta} = -U, \;\; \frac{\partial \psi}{\partial r} = 0, \;\; \theta = 0, \\ \frac{\partial \psi}{\partial \theta} = 0, \;\; \frac{\partial \psi}{\partial r} = 0, \;\; \theta = \theta_0. \end{gathered} \tag{3.5}$$

The Navier-Stokes equation in cylindrical coordinates with a stream function defined as above is given by

$$\nu \nabla_r^4 \psi = -\frac{1}{r}\frac{\partial\left(\psi, \nabla_r^2 \psi\right)}{\partial(r, \theta)}, \tag{3.6}$$

where $\nu = \mu/\rho$ is the kinematic viscosity and ρ is the density, and the Laplacian ∇_r^2 is given by

$$\nabla_r^2 = \frac{\partial^2}{\partial r^2} + \frac{1}{r}\frac{\partial}{\partial r} + \frac{1}{r^2}\frac{\partial^2}{\partial \theta^2}. \tag{3.7}$$

By introducing the dimensionless variables $r^* = r/L,\ \mathbf{v}^* = \mathbf{v}/U,\ \psi^* = \psi/UL$ where L is some characteristic length, the Navier-Stokes equation and no-slip boundary conditions become

$$\begin{gathered}\nabla^4_{r^*}\psi^* = -\frac{R}{r^*}\frac{\partial\left(\psi^*, \nabla^2_{r^*}\psi^*\right)}{\partial\left(r^*, \theta\right)},\\ \frac{1}{r^*}\frac{\partial\psi^*}{\partial\theta} = -1,\ \frac{\partial\psi^*}{\partial r^*} = 0,\ \theta = 0,\\ \frac{\partial\psi^*}{\partial\theta} = 0,\ \frac{\partial\psi^*}{\partial r^*} = 0,\ \theta = \theta_0,\end{gathered} \tag{3.8}$$

where R is the dimensionless Reynolds number defined by $R = UL/\nu$.

Assuming $R \ll 1$ the Navier-Stokes equation reduces to the biharmonic equation $\nabla^4_{r^*}\psi^* = 0$, corresponding to creeping flow. On reverting back to physical variables, assuming a solution of the form $\psi\left(r, \theta\right) = Urf\left(\theta\right)$ implies

$$\frac{d^4 f}{d\theta^4} + 2\frac{d^2 f}{d\theta^2} + f = 0, \tag{3.9}$$

which from Eq. (3.5) is subject to

$$f\left(0\right) = 0, f'\left(0\right) = -1, f\left(\theta_0\right) = 0, f'\left(\theta_0\right) = 0. \tag{3.10}$$

The general solution for $f\left(\theta\right)$ is given by

$$f\left(\theta\right) = C_1\sin\theta + C_2\cos\theta + \theta\left(C_3\sin\theta + C_4\cos\theta\right), \tag{3.11}$$

where throughout C_1, C_2, C_3 and C_4 denote arbitrary integration constants. Applying the boundary conditions yields

$$C_1 = -\frac{\theta_0^2}{\theta_0^2 - \sin^2\theta_0}, C_2 = 0, C_3 = \frac{\theta_0 - \frac{1}{2}\sin 2\theta_0}{\theta_0^2 - \sin^2\theta_0}, C_4 = \frac{\sin^2\theta_0}{\theta_0^2 - \sin^2\theta_0}. \tag{3.12}$$

Hence the classical stream function $\psi\left(r, \theta\right)$ corresponding to no-slip at the boundaries is given by

$$\begin{aligned}\psi\left(r, \theta\right) = \frac{Ur}{\theta_0^2 - \sin^2\theta_0}\left\{\left[\left(\theta_0 - \tfrac{1}{2}\sin 2\theta_0\right)\theta - \theta_0^2\right]\sin\theta\right.\\ \left.+\theta\sin^2\theta_0\cos\theta\right\}.\end{aligned} \tag{3.13}$$

The tangential and normal components of stress may be calculated from $\mathbf{T} = -p\mathbf{I} + 2\mu\mathbf{D}$, where

$$\begin{aligned}T_{rr} &= -p + 2\mu D_{rr} = -p + 2\mu\frac{\partial v_r}{\partial r},\\ T_{r\theta} &= 2\mu D_{r\theta} = \mu\left[r\frac{\partial}{\partial r}\left(\frac{v_\theta}{r}\right) + \frac{1}{r}\frac{\partial v_r}{\partial\theta}\right].\end{aligned} \tag{3.14}$$

The mean pressure p is calculated from the Navier-Stokes equation consistent with the approximation employed, that is neglecting the convective inertial term, which

is given by
r component:

$$\frac{\partial p}{\partial r} = \frac{\mu}{r}\frac{\partial}{\partial \theta}\left[\frac{1}{r}\frac{\partial v_r}{\partial \theta} - \left(\frac{\partial v_\theta}{\partial r} + \frac{v_\theta}{r}\right)\right], \tag{3.15}$$

θ component:

$$\frac{1}{r}\frac{\partial p}{\partial \theta} = -\mu\frac{\partial}{\partial r}\left[\frac{1}{r}\frac{\partial v_r}{\partial \theta} - \left(\frac{\partial v_\theta}{\partial r} + \frac{v_\theta}{r}\right)\right], \tag{3.16}$$

while the z component yields $\partial p/\partial z = 0$. By calculating the r and θ components of velocity from the definition of the stream function and integrating yields the following expression for p

$$p = \frac{2\mu U\left[\left(\theta_0 - \frac{1}{2}\sin 2\theta_0\right)\sin\theta + \sin^2\theta_0\cos\theta\right]}{r\left(\theta_0^2 - \sin^2\theta_0\right)}. \tag{3.17}$$

Substituting this expression and the expressions for the r and θ components of velocity into the expression for T_{rr} and $T_{r\theta}$ yields

$$\begin{aligned} T_{rr} &= -\frac{2\mu U\left[\left(\theta_0 - \frac{1}{2}\sin 2\theta_0\right)\sin\theta + \sin^2\theta_0\cos\theta\right]}{r\left(\theta_0^2 - \sin^2\theta_0\right)}, \\ T_{r\theta} &= \frac{2\mu U\left[\left(\theta_0 - \frac{1}{2}\sin 2\theta_0\right)\cos\theta - \sin^2\theta_0\sin\theta\right]}{r\left(\theta_0^2 - \sin^2\theta_0\right)}. \end{aligned} \tag{3.18}$$

It can immediately be seen that the classical analysis predicts an unphysical stress singularity since $T_{rr} = O\left(r^{-1}\right) = T_{r\theta}$. Thus the distribution of viscous stress along the boundaries involves nonintegrable singularities, leading to a logarithmically infinite force between the fluid and the boundaries. This singularity is a consequence of the imposed discontinuity of velocity at the corner, that is where the fixed and moving boundaries intersect, the velocity variation becomes infinitely fast because two different velocities are assumed along the two boundaries.

The tangential stresses on each boundary may be written

$$T_{r\theta}|_{\theta=0} = \mu U r^{-1}\hat{k}_1,\ T_{r\theta}|_{\theta=\theta_0} = \mu U r^{-1}\hat{k}_2, \tag{3.19}$$

where

$$\hat{k}_1 = \frac{2\left(\theta_0 - \frac{1}{2}\sin 2\theta_0\right)}{\theta_0^2 - \sin^2\theta_0},\ \hat{k}_2 = \frac{2\left(\theta_0\cos\theta_0 - \sin\theta_0\right)}{\theta_0^2 - \sin^2\theta_0}. \tag{3.20}$$

Note that $\hat{k}_1$ and $\hat{k}_2$ depend on θ_0 only, which is an assumed input parameter, and hence are constant.

3.1. Right-angled corner flow

When the boundaries meet at an angle of $\pi/2$, the stream function is given by

$$\psi(r,\theta) = \frac{4Ur}{\pi^2 - 4}\left[\frac{\pi}{2}\left(\theta - \frac{\pi}{2}\right)\sin\theta + \theta\cos\theta\right], \tag{3.21}$$

the pressure is given by $p = -T_{rr}$, and the normal and tangential components of stress become

$$\begin{aligned} T_{rr} &= -\frac{4\mu U\left(\pi \sin\theta + 2\cos\theta\right)}{r\left(\pi^2 - 4\right)}, \\ T_{r\theta} &= \frac{4\mu U\left(\pi \cos\theta - 2\sin\theta\right)}{r\left(\pi^2 - 4\right)}. \end{aligned} \tag{3.22}$$

Then $\hat{k}_1$ and $\hat{k}_2$ are given by

$$\hat{k}_1 = \frac{4\pi}{\pi^2 - 4},\ \hat{k}_2 = -\frac{8}{\pi^2 - 4}. \tag{3.23}$$

4. Navier boundary condition and solution via coupled integral equations

With the Navier boundary condition the relevant boundary conditions are given by

$$\begin{aligned} v_r &= -U + \frac{\ell_1}{r}\frac{\partial v_r}{\partial \theta},\ v_\theta = 0,\ \theta = 0, \\ v_r &= -\frac{\ell_2}{r}\frac{\partial v_r}{\partial \theta},\ v_\theta = 0,\ \theta = \theta_0, \end{aligned} \tag{4.1}$$

where for generality it is assumed that each boundary has a constant but general slip length. In terms of a stream function $\psi\left(r, \theta\right)$ the boundary conditions may be written

$$\begin{aligned} \frac{1}{r}\frac{\partial \psi}{\partial \theta} &= -U + \frac{\ell_1}{r^2}\frac{\partial^2 \psi}{\partial \theta^2},\ \frac{\partial \psi}{\partial r} = 0,\ \theta = 0, \\ \frac{1}{r}\frac{\partial \psi}{\partial \theta} &= -\frac{\ell_2}{r^2}\frac{\partial^2 \psi}{\partial \theta^2},\ \frac{\partial \psi}{\partial r} = 0,\ \theta = \theta_0. \end{aligned} \tag{4.2}$$

To determine the flow near the corner with the Navier boundary condition, we follow closely the analysis of Hocking [8, 9] and define

$$\psi\left(r, \theta\right) = Ur\bar{\psi}\left(\rho, \theta\right), \tag{4.3}$$

where

$$\rho = \ln\left(r/\ell_2\right). \tag{4.4}$$

Then the biharmonic equation $\nabla_r^4 \psi = 0$ becomes

$$\left[\left(\frac{\partial}{\partial \rho} + 1\right)^2 + \frac{\partial^2}{\partial \theta^2}\right]\left[\left(\frac{\partial}{\partial \rho} - 1\right)^2 + \frac{\partial^2}{\partial \theta^2}\right]\bar{\psi} = 0, \tag{4.5}$$

and the boundary conditions may be written

$$\begin{gathered}\bar{\psi}(\rho,0)+\frac{\partial\bar{\psi}}{\partial\rho}(\rho,0)=\bar{\psi}(\rho,\theta_0)+\frac{\partial\bar{\psi}}{\partial\rho}(\rho,\theta_0)=0,\\ \frac{\partial\bar{\psi}}{\partial\theta}(\rho,0)-\tilde{\ell}e^{-\rho}\frac{\partial^2\bar{\psi}}{\partial\theta^2}(\rho,0)=-1,\\ \frac{\partial\bar{\psi}}{\partial\theta}(\rho,\theta_0)+e^{-\rho}\frac{\partial^2\bar{\psi}}{\partial\theta^2}(\rho,\theta_0)=0,\end{gathered}\tag{4.6}$$

where $\tilde{\ell}=\ell_1/\ell_2$.

For the slip solution to reduce to the no-slip solution as $\ell_i\to 0$, that is as $\rho\to\infty$, we must have

$$\bar{\psi}(\infty,\theta)=f(\theta),\tag{4.7}$$

and to ensure that the tangential stress is finite at the origin, that is as $\rho\to-\infty$, we must have

$$\bar{\psi}(\rho,\theta)=O(e^{\rho})\ \text{ as } \rho\to-\infty.\tag{4.8}$$

The tangential stress is given by

$$T_{r\theta}=\frac{\mu U}{r}\left(-\frac{\partial^2\bar{\psi}}{\partial\rho^2}+\bar{\psi}+\frac{\partial^2\bar{\psi}}{\partial\theta^2}\right).\tag{4.9}$$

The tangential stresses on each boundary may be written

$$T_{r\theta}|_{\theta=0}=\mu U r^{-1}k_1(\rho),\ T_{r\theta}|_{\theta=\theta_0}=\mu U r^{-1}k_2(\rho),\tag{4.10}$$

where the derivatives with respect to ρ are zero on the boundaries [7], so that

$$k_1(\rho)=\frac{\partial^2\bar{\psi}}{\partial\theta^2}(\rho,0),\ k_2(\rho)=\frac{\partial^2\bar{\psi}}{\partial\theta^2}(\rho,\theta_0),\tag{4.11}$$

and it is required that

$$\begin{gathered}k_1(\infty)=\hat{k}_1,\ k_2(\infty)=\hat{k}_2,\\ k_1(\rho)=k_2(\rho)=O(e^{\rho})\ \text{ as } \rho\to-\infty.\end{gathered}\tag{4.12}$$

The slip boundary conditions may then be written

$$\begin{gathered}1-\tilde{\ell}e^{-\rho}k_1(\rho)=-\frac{\partial\bar{\psi}}{\partial\theta}(\rho,0),\\ -e^{-\rho}k_2(\rho)=\frac{\partial\bar{\psi}}{\partial\theta}(\rho,\theta_0).\end{gathered}\tag{4.13}$$

We now introduce the two-sided Laplace transform

$$\tilde{\psi}(s,\theta)=\int_{-\infty}^{\infty}e^{-s\rho}\bar{\psi}(\rho,\theta)\,d\rho,\tag{4.14}$$

which has inverse transformation

$$\bar{\psi}(\rho,\theta)=\frac{1}{2\pi i}\int_{\epsilon-i\infty}^{\epsilon+i\infty}e^{s\rho}\tilde{\psi}(s,\theta)\,ds. \tag{4.15}$$

The condition imposed on $\bar{\psi}$ as $\rho\to\infty$ imply $Re(s)>0$, while the condition imposed on $\bar{\psi}$ as $\rho\to-\infty$ imply $Re(s)<1$, thus the transform exists for $0<Re(s)<1$.

The two-sided Laplace transform for the modified biharmonic equation, Eq. (4.5), is

$$\frac{\partial^4\tilde{\psi}}{\partial\theta^4}+2\left(s^2+1\right)\frac{\partial^2\tilde{\psi}}{\partial\theta^2}+\left(s^2-1\right)^2\tilde{\psi}=0, \tag{4.16}$$

which has solution

$$\begin{aligned}\tilde{\psi}(s,\theta)=C_1(s)\sin[(s+1)\theta]+C_2(s)\cos[(s+1)\theta]\\ +C_3(s)\sin[(s-1)\theta]+C_4(s)\cos[(s-1)\theta],\end{aligned} \tag{4.17}$$

where C_i are functions of s to be found. The boundary conditions given by Eq. (4.6a) become

$$\tilde{\psi}(s,0)=\tilde{\psi}(s,\theta_0)=0, \tag{4.18}$$

which imply

$$\tilde{\psi}(s,\theta)=A(s)\sin(s\theta)\sin(\theta-\theta_0)+B(s)\sin[s(\theta-\theta_0)]\sin\theta. \tag{4.19}$$

The boundary conditions given by Eq. (4.11) become

$$\tilde{k}_1(s)=\frac{\partial^2\tilde{\psi}}{\partial\theta^2}(s,0),\ \tilde{k}_2(s)=\frac{\partial^2\tilde{\psi}}{\partial\theta^2}(s,\theta_0), \tag{4.20}$$

where $\tilde{k}_i(s)$ denotes the two-sided Laplace transform of $k_i(\rho)$. Hence

$$\begin{aligned}\tilde{\psi}(s,\theta)=&\frac{\left[\tilde{k}_2(s)\cos(s\theta_0)-\tilde{k}_1(s)\cos\theta_0\right]\sin(s\theta)\sin(\theta-\theta_0)}{2s\left[\cos^2(s\theta_0)-\cos^2\theta_0\right]}\\ &+\frac{\left[\tilde{k}_1(s)\cos(s\theta_0)-\tilde{k}_2(s)\cos\theta_0\right]\sin\theta\sin[s(\theta-\theta_0)]}{2s\left[\cos^2(s\theta_0)-\cos^2\theta_0\right]}.\end{aligned} \tag{4.21}$$

Thus we find

$$\begin{aligned}-\frac{\partial\tilde{\psi}}{\partial\theta}(s,0)=&\frac{\tilde{k}_1(s)\left[\sin(s\theta_0)\cos(s\theta_0)-\frac{1}{2}s\sin 2\theta_0\right]}{2s\left[\cos^2(s\theta_0)-\cos^2\theta_0\right]}\\ &+\frac{\tilde{k}_2(s)\left[s\cos(s\theta_0)\sin\theta_0-\sin(s\theta_0)\cos\theta_0\right]}{2s\left[\cos^2(s\theta_0)-\cos^2\theta_0\right]},\end{aligned} \tag{4.22}$$

$$\frac{\partial\tilde{\psi}}{\partial\theta}(s,\theta_0)=\frac{\tilde{k}_1(s)\left[s\cos(s\theta_0)\sin\theta_0-\sin(s\theta_0)\cos\theta_0\right]}{2s\left[\cos^2(s\theta_0)-\cos^2\theta_0\right]}+\frac{\tilde{k}_2(s)\left[\sin(s\theta_0)\cos(s\theta_0)-\frac{1}{2}s\sin 2\theta_0\right]}{2s\left[\cos^2(s\theta_0)-\cos^2\theta_0\right]}. \quad (4.23)$$

The inversion of these expressions may be written as convolution integrals, so that

$$\begin{aligned}-\frac{\partial\bar{\psi}}{\partial\theta}(\rho,0)&=\int_{-\infty}^{\infty}\left[k_1(u)P(\rho-u)+k_2(u)Q(\rho-u)\right]du,\\ \frac{\partial\bar{\psi}}{\partial\theta}(\rho,\theta_0)&=\int_{-\infty}^{\infty}\left[k_1(u)Q(\rho-u)+k_2(u)P(\rho-u)\right]du,\end{aligned} \quad (4.24)$$

where

$$\begin{aligned}P(\rho)&=\frac{1}{2\pi i}\int_{\epsilon-i\infty}^{\epsilon+i\infty}e^{s\rho}\frac{\sin(s\theta_0)\cos(s\theta_0)-\frac{1}{2}s\sin 2\theta_0}{2s\left[\cos^2(s\theta_0)-\cos^2\theta_0\right]},\\ Q(\rho)&=\frac{1}{2\pi i}\int_{\epsilon-i\infty}^{\epsilon+i\infty}e^{s\rho}\frac{s\cos(s\theta_0)\sin\theta_0-\sin(s\theta_0)\cos\theta_0}{2s\left[\cos^2(s\theta_0)-\cos^2\theta_0\right]},\end{aligned} \quad (4.25)$$

and $0<\epsilon<1$. Substituting Eqs. (4.24) into Eqs. (4.13) yields

$$\begin{aligned}1-\tilde{\ell}e^{-\rho}k_1(\rho)&=\int_{-\infty}^{\infty}\left[k_1(u)P(\rho-u)+k_2(u)Q(\rho-u)\right]du,\\ -e^{-\rho}k_2(\rho)&=\int_{-\infty}^{\infty}\left[k_1(u)Q(\rho-u)+k_2(u)P(\rho-u)\right]du.\end{aligned} \quad (4.26)$$

If we write $F_1(r)$ and $F_2(r)$ for the force on each of the boundaries then

$$\begin{aligned}F_1(r)&=\int_0^r T_{r\theta}|_{\theta=0}dr=\mu U\int_{-\infty}^{\ln(r/\ell)}k_1(\rho)\,d\rho,\\ F_2(r)&=\int_0^r T_{r\theta}|_{\theta=\theta_0}dr=\mu U\int_{-\infty}^{\ln(r/\ell)}k_2(\rho)\,d\rho.\end{aligned} \quad (4.27)$$

Thus for any set of values of the parameters θ_0 and $\tilde{\ell}$ Eqs. (4.26) represent a set of coupled integral equations for the unknowns $k_1(\rho)$ and $k_2(\rho)$. These may be solved numerically for $k_1(\rho)$ and $k_2(\rho)$ and applied to Eq. (4.27) to obtain the force on each boundary.

5. Solution for right-angled corner flow

When the boundaries meet at an angle of $\theta_0=\pi/2$ and when the slip lengths for each boundary are equal, that is $\tilde{\ell}=1$, the integral equations given by Eq. (4.26)

become

$$\begin{aligned} 1-e^{-\rho}k_1(\rho) &= \int_{-\infty}^{\infty}\left[k_1(u)\,P(\rho-u)+k_2(u)\,Q(\rho-u)\right]du, \\ -e^{-\rho}k_2(\rho) &= \int_{-\infty}^{\infty}\left[k_1(u)\,Q(\rho-u)+k_2(u)\,P(\rho-u)\right]du, \end{aligned} \tag{5.1}$$

where

$$\begin{aligned} P(\rho) &= \frac{1}{2\pi i}\int_{\epsilon-i\infty}^{\epsilon+i\infty} e^{s\rho}\frac{\tan(\pi s/2)}{2s}ds = \frac{1}{2\pi}\ln\left|\frac{1+e^{-|\rho|}}{1-e^{-|\rho|}}\right|, \\ Q(\rho) &= \frac{1}{2\pi i}\int_{\epsilon-i\infty}^{\epsilon+i\infty} e^{s\rho}\frac{\sec(\pi s/2)}{2}ds = \frac{1}{2\pi\cosh(\rho)}. \end{aligned} \tag{5.2}$$

If we define $k_1+k_2=k_a$ and $k_1-k_2=k_b$ then the above integral equations may be uncoupled by addition to give

$$1-e^{-\rho}k_a(\rho) = \int_{-\infty}^{\infty}\left[P(\rho-u)+Q(\rho-u)\right]k_a(u)\,du, \tag{5.3}$$

and subtraction to give

$$1-e^{-\rho}k_b(\rho) = \int_{-\infty}^{\infty}\left[P(\rho-u)-Q(\rho-u)\right]k_b(u)\,du. \tag{5.4}$$

Thus we must solve two independent integral equations. To the author's knowledge an exact analytical solution is possible only for $Q(\rho)=0$ (see Hocking [8, 9]).

5.1. Numerical solution

The function $P(\rho-u)$ has a logarithmic singularity at $\rho=u$, which may be removed by noting that Eqs. (5.3) and (5.4) may be written

$$\begin{aligned} 1-e^{-\rho}k_a(\rho) = &\int_{-\infty}^{\infty}\left[P(\rho-u)+Q(\rho-u)\right]\left[k_a(u)-k_a(\rho)\right]du \\ &+k_a(\rho)\int_{-\infty}^{\infty}\left[P(\rho-u)+Q(\rho-u)\right]du, \end{aligned} \tag{5.5}$$

and

$$\begin{aligned} 1-e^{-\rho}k_b(\rho) = &\int_{-\infty}^{\infty}\left[P(\rho-u)-Q(\rho-u)\right]\left[k_b(u)-k_b(\rho)\right]du \\ &+k_b(\rho)\int_{-\infty}^{\infty}\left[P(\rho-u)-Q(\rho-u)\right]du. \end{aligned} \tag{5.6}$$

It follows from Eq. (5.2) that

$$\begin{aligned}\int_{-\infty}^{\infty}\left[P\left(\rho-u\right)+Q\left(\rho-u\right)\right]du&=\hat{k}_a^{-1},\\ \int_{-\infty}^{\infty}\left[P\left(\rho-u\right)-Q\left(\rho-u\right)\right]du&=\hat{k}_b^{-1}.\end{aligned}\tag{5.7}$$

where

$$\hat{k}_a=\hat{k}_1+\hat{k}_2=\frac{4}{\pi+2},\ \hat{k}_b=\hat{k}_1-\hat{k}_2=\frac{4}{\pi-2}\tag{5.8}$$

Hence the integral equations to be solved are

$$\begin{aligned}1-\left(e^{-\rho}+\frac{\pi+2}{4}\right)k_a\left(\rho\right)&\\ =\int_{-\infty}^{\infty}\left[P\left(\rho-u\right)+Q\left(\rho-u\right)\right]\left[k_a\left(u\right)-k_a\left(\rho\right)\right]du,&\end{aligned}\tag{5.9}$$

and

$$\begin{aligned}1-\left(e^{-\rho}+\frac{\pi-2}{4}\right)k_b\left(\rho\right)&\\ =\int_{-\infty}^{\infty}\left[P\left(\rho-u\right)-Q\left(\rho-u\right)\right]\left[k_b\left(u\right)-k_b\left(\rho\right)\right]du.&\end{aligned}\tag{5.10}$$

The numerical method used to solve the integral equations Eqs. (5.9) and (5.10) is to define the functions $k_a\left(\rho\right)$ and $k_b\left(\rho\right)$ by their values at a set of equally spaced points in the finite interval $-N$ to N, and evaluate the integral using the trapezoidal rule. The resulting set of $2N+1$ linear equations for each $k_a\left(\rho\right)$ and $k_b\left(\rho\right)$ are then solved numerically for the function values. The results are plotted in Fig. 1, where

$$k_1=\frac{k_a+k_b}{2},\ k_2=\frac{k_a-k_b}{2}.\tag{5.11}$$

Numerical calculations imply that for a large enough N we have $k_i\left(\rho\right)\approx 0$ for $\rho<-N$ and $k_i\left(\rho\right)\approx\hat{k}_i$ for $\rho>N$, so that for $\ln\left(r/\ell\right)>N$ the integral given by Eq. (4.27) may be written

$$\begin{aligned}F_i\left(r\right)=\mu U\int_{-\infty}^{\ln(r/\ell)}k_i\left(\rho\right)d\rho&\approx\mu U\left[\int_{-N}^{N}k_i\left(\rho\right)d\rho+\hat{k}_i\int_{N}^{\ln(r/\ell)}d\rho\right]\\ &=\mu U\left\{\int_{-N}^{N}k_i\left(\rho\right)d\rho+\hat{k}_i\left[\ln\left(r/\ell\right)-N\right]\right\}\\ &=\mu U\left[\hat{k}_i\ln\left(r/\ell\right)+h_i\right],\end{aligned}\tag{5.12}$$

where

$$h_i=\int_{-N}^{N}k_i\left(\rho\right)d\rho-N\hat{k}_i,\tag{5.13}$$

may also be evaluated by the trapezoidal rule. From numerical calculation we find that

$$h_a = 0.312,\ h_b = -4.344, \tag{5.14}$$

hence

$$h_1 = \frac{h_a + h_b}{2} = -2.016,\ h_2 = \frac{h_a - h_b}{2} = 2.328. \tag{5.15}$$

5.2. Approximate analytical solution

Appendix A outlines an approximate analytical solution for $k_a(\rho)$ and $k_b(\rho)$, which are

$$\begin{aligned} k_a(\rho) = \frac{2e^{\rho}}{\pi} \Bigg\{ & \mathrm{Ci}\left[\frac{(\pi+2)\,e^{\rho}}{2\pi}\right] \sin\left[\frac{(\pi+2)\,e^{\rho}}{2\pi}\right] \\ & -\mathrm{si}\left[\frac{(\pi+2)\,e^{\rho}}{2\pi}\right] \cos\left[\frac{(\pi+2)\,e^{\rho}}{2\pi}\right] \Bigg\}, \end{aligned} \tag{5.16}$$

and

$$\begin{aligned} k_b(\rho) = \frac{2e^{\rho}}{\pi} \Bigg\{ & \mathrm{Ci}\left[\frac{(\pi-2)\,e^{\rho}}{2\pi}\right] \sin\left[\frac{(\pi-2)\,e^{\rho}}{2\pi}\right] \\ & -\mathrm{si}\left[\frac{(\pi-2)\,e^{\rho}}{2\pi}\right] \cos\left[\frac{(\pi-2)\,e^{\rho}}{2\pi}\right] \Bigg\}, \end{aligned} \tag{5.17}$$

where Ci and si are the cosine and sine integrals as defined in Abramowitz and Stegun [1] and given by

$$\mathrm{Ci}(x) = -\int_x^{\infty} \frac{\cos t}{t} dt,\ \mathrm{si}(x) = -\int_x^{\infty} \frac{\sin t}{t} dt. \tag{5.18}$$

As can be verified from numerical calculations,

$$\begin{gathered} k_a(\infty) = \hat{k}_a,\ k_b(\infty) = \hat{k}_b, \\ k_a(\rho) = k_b(\rho) = O(e^{\rho}) \ \text{ as } \rho \to -\infty. \end{gathered} \tag{5.19}$$

Comparisons of the numerical solution and these approximate analytical solutions are shown in Table 1 and compared graphically in Fig. 2, which show excellent agreement. From these approximate analytical solutions we may deduce the finite expressions for the force on each boundary as a function of $r > 0$ and $\ell > 0$ from Eq. (4.27)

$$\begin{aligned} F_a(r) = \frac{4\mu U}{\pi+2} \Bigg\{ & \ln\left(\frac{r}{\ell}\right) - \mathrm{Ci}\left[\frac{(\pi+2)\,r}{2\pi\ell}\right] \cos\left[\frac{(\pi+2)\,r}{2\pi\ell}\right] \\ & -\mathrm{si}\left[\frac{(\pi+2)\,r}{2\pi\ell}\right] \sin\left[\frac{(\pi+2)\,r}{2\pi\ell}\right] + \gamma - \ln 2 + \ln\left(\frac{\pi+2}{\pi}\right) \Bigg\}, \end{aligned} \tag{5.20}$$

and

$$F_b(r) = \frac{4\mu U}{\pi - 2}\left\{\ln\left(\frac{r}{\ell}\right) - \mathrm{Ci}\left[\frac{(\pi-2)\,r}{2\pi\ell}\right]\cos\left[\frac{(\pi-2)\,r}{2\pi\ell}\right] - \mathrm{si}\left[\frac{(\pi-2)\,r}{2\pi\ell}\right]\sin\left[\frac{(\pi-2)\,r}{2\pi\ell}\right] + \gamma - \ln 2 + \ln\left(\frac{\pi-2}{\pi}\right)\right\}, \tag{5.21}$$

where γ is the Euler-Masheroni constant. Note that $F_1 = (F_a + F_b)/2$ and $F_2 = (F_a - F_b)/2$.

From the above expressions approximate values of h_a and h_b may be found by taking the limit $r/\ell \to \infty$ and comparing Eq. (4.27) with Eq. (5.12). Equation (5.18) implies that $\mathrm{Ci}(x)$ and $\mathrm{si}(x)$ approach 0 as $x \to \infty$, hence we find that

$$h_a = \frac{4}{\pi+2}\left[\gamma - \ln 2 + \ln\left(\frac{\pi+2}{\pi}\right)\right] = 0.293,$$
$$h_b = \frac{4}{\pi-2}\left[\gamma - \ln 2 + \ln\left(\frac{\pi-2}{\pi}\right)\right] = -3.953, \tag{5.22}$$

which are in relative agreement with the numerical results given by Eq. (5.14).

6. Solution away from the corner

Assuming a similarity solution which is slightly more general than the classical solution of the form $\psi(r,\theta) = U[r f_1(\theta) + f_2(\theta)]$ splits the problem into two parts. The solution $f_1(\theta)$ corresponds to the classical solution, while the solution $f_2(\theta)$ satisfies

$$\frac{d^4 f_2}{d\theta^4} + 4\frac{d^2 f_2}{d\theta^2} = 0, \tag{6.1}$$

which from Eq. (4.1) is subject to

$$f_2'(0) = \ell_1 f_1''(0),\ f_2''(0) = 0,\ f_2'(\theta_0) = -\ell_2 f_1''(\theta_0),\ f_2''(\theta_0) = 0. \tag{6.2}$$

The general solution for $f_2(\theta)$ is given by

$$f_2(\theta) = C_1 + C_2\theta + C_3\sin 2\theta + C_4\cos 2\theta, \tag{6.3}$$

and applying the boundary conditions yields two distinct cases, which are outlined below.

6.1. Solution for arbitrary θ_0

For an arbitrary contact angle between the boundaries it is required that $\ell_2 = [(\theta_0 - \sin\theta_0\cos\theta_0)/(\sin\theta_0 - \theta_0\cos\theta_0)]\,\ell_1$, and we find

$$f_2(\theta) = C_1 + \frac{2\ell_1\left(\theta_0 - \frac{1}{2}\sin 2\theta_0\right)}{\theta_0^2 - \sin^2\theta_0}\theta. \tag{6.4}$$

Hence the stream function is given by $\psi(r,\theta) = \psi_1(r,\theta) + \psi_2(r,\theta)$, where $\psi_1(r,\theta)$ is given by the classical solution and $\psi_2(r,\theta)$ is given by $\psi_2(r,\theta) = Uf_2(\theta)$, with an arbitrary constant C_1, which may be set to zero without loss of generality.

The pressure and tangential and normal components of stress are given by $p = p_1 + p_2$, $T_{rr} = T_{rr1} + T_{rr2}$ and $T_{r\theta} = T_{r\theta 1} + T_{r\theta 2}$, where p_1, T_{rr1} and $T_{r\theta 1}$ are given by the classical solution, and

$$\begin{aligned} p_2 &= 0 = T_{r\theta 2}, \\ T_{rr2} &= -\frac{4\mu U \ell_1 \left(\theta_0 - \frac{1}{2}\sin 2\theta_0\right)}{r^2\left(\theta_0^2 - \sin^2\theta_0\right)}. \end{aligned} \tag{6.5}$$

6.2. Solution for right-angled corner flow

When the boundaries meet at an angle of $\theta_0 = \pi/2$ we find

$$f_2(\theta) = C_1 + \frac{2(\pi\ell_1 + 2\ell_2)\theta}{\pi^2 - 4} + \frac{(\pi\ell_1 - 2\ell_2)\sin 2\theta}{\pi^2 - 4}. \tag{6.6}$$

Hence the stream function is given by $\psi(r,\theta) = \psi_1(r,\theta) + \psi_2(r,\theta)$, where $\psi_1(r,\theta)$ is given by the classical solution with $\theta_0 = \pi/2$ and $\psi_2(r,\theta)$ is given by $\psi_2(r,\theta) = Uf_2(\theta)$, with an arbitrary constant C_1, which may be set to zero without loss of generality

The pressure and tangential and normal components of stress are given by $p = p_1 + p_2$, $T_{rr} = T_{rr1} + T_{rr2}$ and $T_{r\theta} = T_{r\theta 1} + T_{r\theta 2}$, where p_1, T_{rr1} and $T_{r\theta 1}$ are given by the classical solution with $\theta_0 = \pi/2$ and

$$\begin{aligned} p_2 &= \frac{4\mu U(\pi\ell_1 - 2\ell_2)\cos 2\theta}{r^2(\pi^2 - 4)}, \\ T_{rr2} &= -\frac{4\mu U\left[2(\pi\ell_1 - 2\ell_2)\cos 2\theta + \pi\ell_1 + 2\ell_2\right]}{r^2(\pi^2 - 4)}, \\ T_{r\theta 2} &= -\frac{4\mu U(\pi\ell_1 - 2\ell_2)\sin 2\theta}{r^2(\pi^2 - 4)}. \end{aligned} \tag{6.7}$$

It can be seen that this analysis predicts a further singularity since $T_{rr2} = O\left(r^{-2}\right) = T_{r\theta 2}$, which as a consequence implies a singularity in the r component of velocity since $v_r = O\left(r^{-1}\right)$. This confirms that the solution is valid away from the corner. Also note that $T_{r\theta 2}|_{\theta=0} = 0 = T_{r\theta 2}|_{\theta=\pi/2}$, that is the similarity solution far from the corner makes no contribution to the tangential stress on the boundaries to that of the classical solution.

When $\ell_1 = \ell_2 = \ell$ the above expressions reduce to

$$\begin{aligned} f_2(\theta) &= \frac{2\ell\theta}{\pi - 2} + \frac{\ell \sin 2\theta}{\pi + 2}, \\ p_2 &= \frac{4\mu U \ell \cos 2\theta}{r^2(\pi + 2)}, \\ T_{rr2} &= -\frac{4\mu U \ell \left[2(\pi - 2)\cos 2\theta + \pi + 2\right]}{r^2(\pi^2 - 4)}, \\ T_{r\theta 2} &= -\frac{4\mu U \ell \sin 2\theta}{r^2(\pi + 2)}. \end{aligned} \tag{6.8}$$

Streamline plots for $\ell = 1$ and $\ell = 2$ are shown in Figs. 3 and 4 for the cases $\psi = -0.5$ and $\psi = -0.1$, respectively (exaggerated values of ℓ are chosen so that each curve is clearly distinguishable).

6.3. Comparison of radial velocities

Although accurate streamline profiles cannot be obtained easily for the integral transform solution, it is however possible to compare the radial component of velocity values for $\theta_0 = \pi/2$, $\theta = \pi/4$ and $\ell_1 = \ell_2 = \ell$ as a function of $r^* \equiv r/\ell$ for the similarity and integral transform solutions. For the similarity solution we have

$$\frac{v_r(r^*, \pi/4)}{U} = \frac{1}{Ur}\frac{\partial \psi}{\partial \theta} = -\frac{\sqrt{2}(\pi - 4)}{4(\pi - 2)} + \frac{2}{r^*(\pi - 2)}, \tag{6.9}$$

while Appendix B gives the equivalent expression, using the approximate analytical expression for k_b given by Eq. (5.17), for the integral transform solution

$$\begin{aligned} \frac{v_r(r^*, \pi/4)}{U} = -\frac{\sqrt{2}}{4\pi^2}\int_0^\infty \frac{r^*}{u^2}\left[\ln\left(\frac{u^2 + \sqrt{2}u + 1}{u^2 - \sqrt{2}u + 1}\right) - \frac{2\sqrt{2}u\left(u^2 + 1\right)}{u^4 + 1}\right] \\ \times\left\{\mathrm{Ci}\left[\frac{(\pi - 2)r^*}{2\pi u}\right]\sin\left[\frac{(\pi - 2)r^*}{2\pi u}\right] \right. \\ \left. -\mathrm{si}\left[\frac{(\pi - 2)r^*}{2\pi u}\right]\cos\left[\frac{(\pi - 2)r^*}{2\pi u}\right]\right\} du, \end{aligned} \tag{6.10}$$

which may be evaluated numerically using MAPLE. The results of the calculations are shown in Figs. 5 and 6 for two ranges of r^*. It can be immediately seen that for low values of r^* there is a significant difference between the values of $v_r(r^*, \pi/4)$, since Eq. (6.9) approaches infinity and Eq. (6.10) approaches zero as $r^* \to 0$. As r^* increases the similarity solution approaches the constant value of $v_r(r^*, \pi/4)$ for the classical solution from above as $r^* \to \infty$, while the integral transfrom solution approaches the constant value of $v_r(r^*, \pi/4)$ for the classical solution from below as $r^* \to \infty$. Thus in the limit $r^* \to \infty$ (that is, $\ell \to 0$) the two solutions agree,

Table 1. Numerical and approximate analytical values of k_a and k_b as determined by Eqs. (5.9), (5.10) and Eqs. (5.16), (5.17) for $-10 \leq \rho \leq 10$.

	Numerical		Analytical	
ρ	k_a	k_b	k_a	k_b
-10	0.000	0.000	0.000	0.000
-9	0.000	0.000	0.000	0.000
-8	0.000	0.000	0.000	0.000
-7	0.001	0.001	0.001	0.001
-6	0.002	0.002	0.002	0.002
-5	0.007	0.007	0.007	0.007
-4	0.017	0.018	0.018	0.018
-3	0.045	0.049	0.045	0.048
-2	0.108	0.130	0.110	0.127
-1	0.237	0.331	0.239	0.318
0	0.439	0.772	0.440	0.739
1	0.646	1.527	0.638	1.496
2	0.755	2.390	0.744	2.457
3	0.777	3.005	0.772	3.171
4	0.778	3.307	0.777	3.440
5	0.778	3.430	0.778	3.494
6	0.778	3.476	0.778	3.503
7	0.778	3.494	0.778	3.504
8	0.778	3.500	0.778	3.504
9	0.778	3.503	0.778	3.504
10	0.778	3.504	0.778	3.504

confirming the findings of the previous sections that away from the corner the similarity and integral transform solutions agree for any finite ℓ.

7. Discussion and concluding remarks

For the integral transform solution the numerical and approximate analytical results for the tangential stress on each boundary for the case $\theta_0 = \pi/2$ and $\ell_1 = \ell_2 = \ell$ are shown in Table 1, and are plotted in Figs. 1 and 2. Examination of Fig. 1 reveals that for a large enough $\rho \equiv \ln(r/\ell)$ the tangential stress on each boundary coincides with that of the classical no-slip solution. Numerical calculations reveal that for a non-zero slip length ℓ, the force on each boundary is finite and approximate analytical expressions for calculating these forces may be obtained from Eqs. (5.20) and (5.21). These findings support those of Hocking [8, 9], that is that a non-zero slip length is capable of removing the non-integrable stress singularity that occurs in many fluid mechanics problems, particularly for the sliding plate and moving contact line problems.

For the similarity solution, the streamline plots for the case $\theta_0 = \pi/2$ and $\ell_1 = \ell_2 = \ell$ are shown in Figs. 3 and 4 for the cases $\psi = -0.5$ and $\psi = -0.1$ for various values of ℓ. Note that the flow is reversible; that is, if U is replaced with $-U$ then identical streamline patterns are obtained with ψ replaced with $-\psi$. These streamline plots are similar to the results obtained by Hancock et al. [6] in

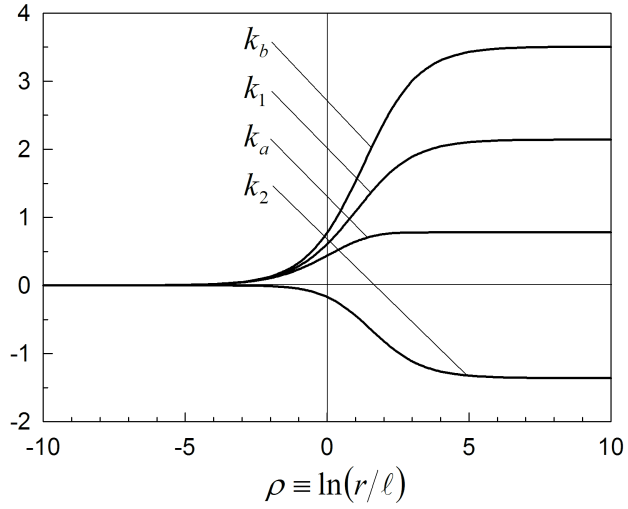

Figure 1. Numerical values of k_a, k_b, k_1 and k_2 for $\theta_0 = \pi/2$ and equal slip lengths $\ell_1 = \ell_2 = \ell$.

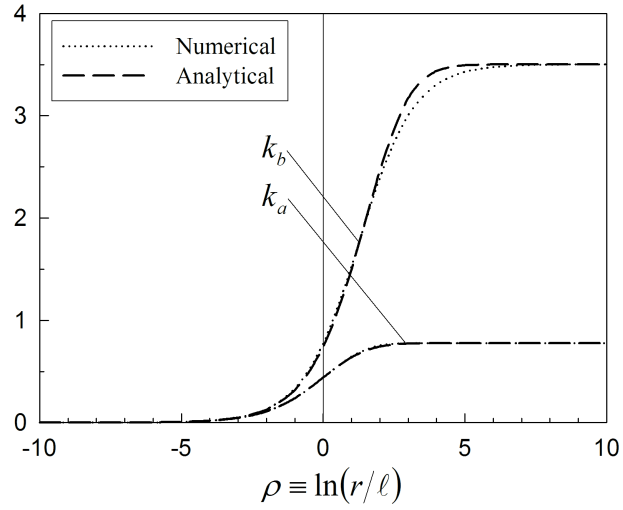

Figure 2. Comparison of numerical and approximate analytical values of k_a and k_b as given by Eqs. (5.9), (5.10) and Eqs. (5.16), (5.17) for $\theta = \pi/2$ and equal slip lengths $\ell_1 = \ell_2 = \ell$.

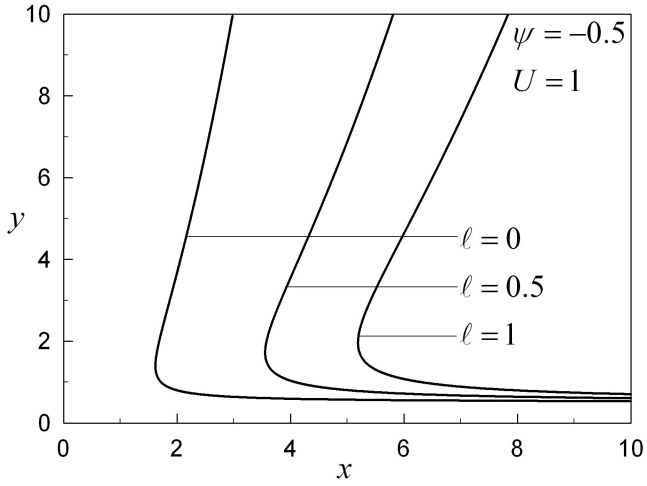

Figure 3. Streamlines for the similarity solution for $\theta_0 = \pi/2$, $\psi = -0.5$, $U = 1$ for various values of the slip length $\ell_1 = \ell_2 = \ell$.

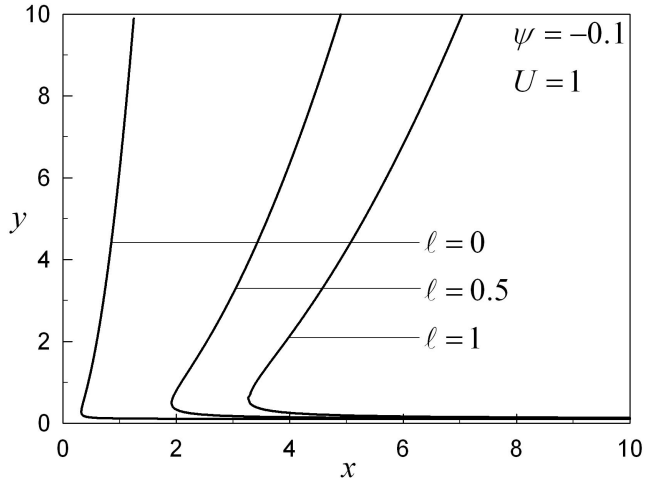

Figure 4. Streamlines for the similarity solution for $\theta_0 = \pi/2$, $\psi = -0.1$, $U = 1$ for various values of the slip length $\ell_1 = \ell_2 = \ell$.

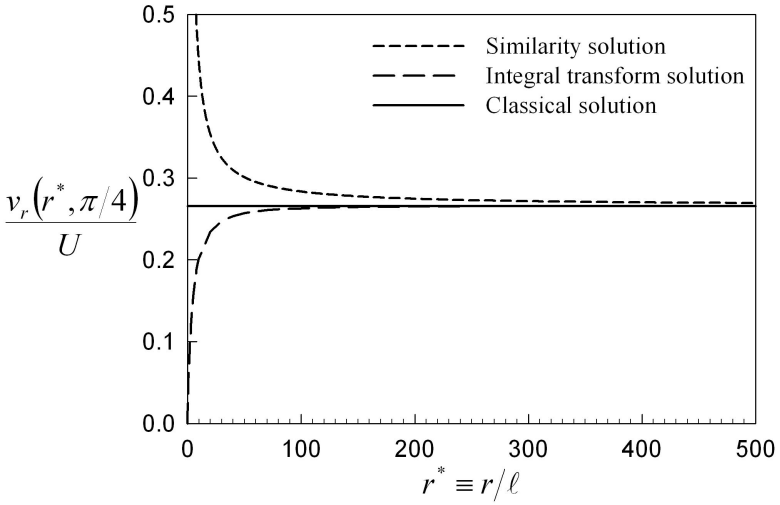

Figure 5. Comparison of radial components of velocity as given by Eqs. (6.9) and (6.10) for the similarity and integral transform solutions for $\theta_0 = \pi/2$ and $\theta = \pi/4$ for various values of $r^* \equiv r/\ell$. The constant radial component of velocity for the classical solution is also plotted for comparison.

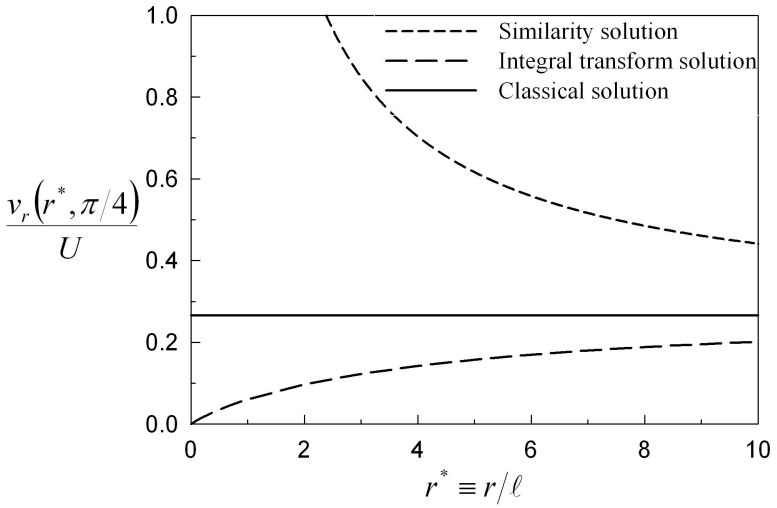

Figure 6. Comparison of radial components of velocity as given by Eqs. (6.9) and (6.10) for the similarity and integral transform solutions for $\theta_0 = \pi/2$ and $\theta = \pi/4$ for various values of $r^* \equiv r/\ell$. The constant radial component of velocity for the classical solution is also plotted for comparison.

their study of the effects of inertia in the sliding plate problem for the case $-U$; that is, the streamline patterns for nonzero ℓ are moved in the opposite direction to those where the effects of inertia are included.

Concerning the tangential stress on the boundary, the results of the similarity solution away from the corner, Eq. (6.8d), imply that the stress is equal to that of the classical solution; that is, the similarity solution away from the corner makes no additional contribution to the tangential stress on the boundaries. This is in agreement with the integral transform solution, which implies for large enough ρ the stress is equal the classical solution. Ideally, we would like to compare the streamlines for both the integral transform solution and the similarity solution. However, this is not straight forward, and instead we calculate the radial component of velocity for the two solutions along the line $\theta = \pi/4$ for increasing distance from the corner. These are shown in Figs. 5 and 6, and confirm that for a sufficient distance from the corner, the two solutions indeed agree.

The nature of the Navier boundary condition on each boundary makes it difficult to obtain a solution to the biharmonic equation which is valid everywhere. The similarity solution is valid away from the corner, but the solution near the corner cannot be obtained explicitly by separation of variables, and only the tangential stress on each boundary may be obtained, and then only either numerically or by an approximate analytical solution, which turns out to be very accurate. A more complicated problem is that of the so-called lid-driven cavity, which has been extensively studied by Shankar [28, 29, 30], Shankar et al. [31], Meleshko [19, 17, 18], Meleshko et al. [20, 21] and Gomilko et al. [4]. This problem involves a two-dimensional creeping flow of a Newtonian fluid in a rectangular cavity, where the motion is produced by applying constant but general velocities on the top and bottom walls. Although more complicated, the problem is usually studied in Cartesian coordinates, and solved using Fourier series. The advantage of studying such a problem is that, as demonstrated by Meleshko [19], the stream function near the corner points may be inferred by locally expanding the full solution in terms of suitably defined polar coordinates. For the no-slip boundary condition, the solutions obtained correspond to the classical solution stated earlier, along with higher-order terms identical to those obtained by Krasnopolskaya [12] and Moffatt [22]. The Navier boundary condition in Cartesian coordinates provides less restrictions on a similarity solution than that in cylindrical coordinates, making the problem more tractable; in particular it may provide more accurate streamline behavior near the corner than the solution obtained here.

Acknowledgements

This work is funded by the Discovery Project scheme of the Australian Research Council, and the authors gratefully acknowledge this support. The authors are also grateful to Tie-Zheng Qian for helpful discussions and drawing their attention

to the problem, and Leslie M. Hocking for helpful correspondence.

References

[1] M. Abramowitz and I. A. Stegun, *Handbook of Mathematical Functions* (Dover Publications Incorporated, New York 1964).
[2] G. K. Batchelor, *An Introduction to Fluid Dynamics* (Cambridge University Press, Cambridge 2000).
[3] V. E. B. Dussan, The moving contact line: the slip boundary condition, *J. Fluid Mech.* **77** (1976) 665–684.
[4] A. M. Gomilko, V. S. Malyuga and V. V. Meleshko, On steady Stokes flow in a trihedral rectangular corner, *J. Fluid Mech.* **476** (2003) 159–177.
[5] J. N. Goodier, An analogy between the slow motion of a viscous fluid in two dimensions, and systems of plane stress, *Phil. Mag.* **17** (1934) 554–576.
[6] C. Hancock, E. Lewis and H. K. Moffatt, Effects of inertia in forced corner flows, *J. Fluid Mech.* **112** (1981) 315–327.
[7] J. Happel and H. Brenner, *Low Reynolds Number Hydrodynamics* (Prentice-Hall, New Jersey 1965).
[8] L. M. Hocking, A moving fluid interface on a rough surface, *J. Fluid Mech.* **76** (1976) 801–817.
[9] L. M. Hocking, A moving fluid interface. Part 2. the removal of the force singularity by a slip flow, *J. Fluid Mech.*, **79** (1977) 209–229.
[10] C. Huh and L. E. Scriven, Hydrodynamic model of steady movement of a solid/liquid/fluid contact line, *J. Colloid Interface Sci.* **35** (1971) 85–101.
[11] J. Koplik and J. R. Banavar, Corner flow in the sliding plate problem, *Phys. Fluids* **7** (1995) 3118–3125.
[12] T. S. Krasnopolskaya, Two-dimensional Stokes flow near a corner in a right angle wedge and Moffatt's eddies, *Mech. Res. Comm.* **22** (1995) 9–14.
[13] H. Lamb, *Hydrodynamics* (Cambridge University Press, Cambridge 1932).
[14] E. Lauga, M. P. Brenner and H. A. Stone, Microfluidics: the no-slip boundary condition *Handbook of Experimental Data, Ch. 15* (Springer, New York 2005).
[15] M. T. Matthews and J. M. Hill, Flow around nanospheres and nanocylinders, *Quart. J. Mech. App. Math.* accepted for publication.
[16] J. C. Maxwell, On stresses in rarefied gases arising from inequalities of temperature, *Phil. Trans. Roy. Soc. Lond.* **170** (1879) 231–256.
[17] V. V. Meleshko, Biharmonic problem in a rectangle, *Appl. Sci. Res.* **58** (1998) 217–249.
[18] V. V. Meleshko, Selected topics in the history of the two-dimensional biharmonic problem, *Appl. Mech. Rev.* **56** (2003) 33–85.
[19] V. V. Meleshko, Steady Stokes flow in a rectangular cavity, *Proc. R. Soc. Lond. A* **452** (1996) 1999–2022.
[20] V. V. Meleshko and A. M. Gomilko, Infinite systems for a biharmonic problem in a rectangle, *Proc. R. Soc. Lond. A* **453** (1997) 2139–2160.
[21] V. V. Meleshko, V. S. Malyuga and A. M. Gomilko, Steady Stokes flow in a finite cylinder, *Proc. R. Soc. Lond. A* **456** (2000) 1741–1758.
[22] H. K. Moffatt, Viscous and resistive eddies near a sharp corner, *J. Fluid Mech.* **18** (1963) 1–18.
[23] C. L. M. H. Navier, Mémoire sur les lois du mouvement des fluides, *Mémoires de l'Académie Royale des Sciences de l'Institut de France* **VI** (1823) 389–440.
[24] T. Qian and X. P. Wang, Driven cavity flow: from molecular dynamics to continuum hydrodynamics, *Mult. Mod. Sim.* **3** (2005) 749–763.

[25] T. Qian, X. P. Wang and P. Sheng, Generalized Navier boundary condition for the moving contact line, *Comm. Math. Sci.* **1** (2003) 333–341.
[26] T. Qian, X. P. Wang and P. Sheng, Molecular scale contact line hydrodynamics of immiscible flows, *Phys. Rev. E* **68** (2003) 1–15.
[27] T. Qian, X. P. Wang and P. Sheng, Power-law slip profile of the moving contact line in two-phase immiscible flows, *Phys. Rev. Lett.* **93** (2004) 1–4.
[28] P. N. Shankar, On Stokes flow in a semi-infinite wedge, *J. Fluid Mech.* **422** (2000) 69–90.
[29] P. N. Shankar, The eddy structure in Stokes flow in a cavity, *J. Fluid Mech.* **250** (2000) 371–383.
[30] P. N. Shankar, Three-dimensional eddy structure in a cylindrical container, *J. Fluid Mech.* **342** (1997) 97–118.
[31] P. N. Shankar and M. D. Deshpande, Fluid mechanics in the driven cavity, *Ann. Rev. Fluid Mech.* **32** (2000) 93–136.
[32] Y. D. Shikhmurzaev, Moving contact lines in liquid/liquid/solid systems, *J. Fluid Mech.* **334** (1997) 211–249.
[33] Y. D. Shikhmurzaev, The moving contact line on a smooth solid surface, *Int. J. Mult. Flow* **19** (1993) 589–610.
[34] J. C. Slattery, *Advanced Transport Phenomena* (Cambridge University Press, Cambridge 1999).
[35] G. I. Taylor, On scraping viscous fluid from a plane surface, *The Scientific Papers of Sir Geoffrey Ingram Taylor, Volume 4 - Mechanics of Fluids: Miscellaneous Papers*, edited by G. K. Batchelor (Cambridge University Press, London 1958).
[36] P. A. Thompson and S. M. Troian, A general boundary condition for liquid flow at solid surfaces, *Nature* **389** (1997) 360–362.

A. Appendix - Approximate analytical solution

Consider the integral equation

$$1 - e^{-\rho} k_\epsilon(\rho) = \frac{1}{2\pi} \int_{-\infty}^{\infty} \left\{ \ln \left| \frac{1 + e^{-|\rho+u|}}{1 - e^{-|\rho+u|}} \right| + \frac{\epsilon}{\cosh(\rho - u)} \right\} k_\epsilon(u)\, du, \qquad \text{(A.1)}$$

where $\epsilon = 1$ for $k_\epsilon = k_a$ and $\epsilon = -1$ for $k_\epsilon = k_b$. When $\epsilon = 0$ Eq. (A.1) reduces to that of Hocking [8, 9], which has an analytical solution given by

$$\begin{aligned} k_0(\rho) &= \frac{4e^\rho}{\pi} \int_0^\infty \frac{\sin(se^\rho)}{1+2s} ds \\ &= \frac{2e^\rho}{\pi} \left[\mathrm{Ci}\left(\tfrac{1}{2}e^\rho\right) \sin\left(\tfrac{1}{2}e^\rho\right) - \mathrm{si}\left(\tfrac{1}{2}e^\rho\right) \cos\left(\tfrac{1}{2}e^\rho\right) \right], \end{aligned} \qquad \text{(A.2)}$$

which can be verified by direct substitution, where Ci and si are the cosine and sine integrals as defined in Abramowitz and Stegun [1]. Hence we assume that k_ϵ has the form

$$k_\epsilon(\rho) = \frac{4e^\rho}{\pi} \int_0^\infty A_\epsilon(s) \sin(se^\rho)\, ds, \qquad \text{(A.3)}$$

where $A_\epsilon(s)$ is a function of s to be found for $\epsilon = \pm 1$, with the property that $A_\epsilon(s) \to 0$ as $s \to \infty$. For $\epsilon = 0$, $A_\epsilon(s)$ reduces to

$$A_0(s) = \frac{1}{1+2s}. \qquad \text{(A.4)}$$

Substituting Eq. (A.3) into (A.1) and rearranging yields

$$\int_0^\infty \frac{A_\epsilon(s)(1+2s)\sin(se^\rho)}{s}ds + \epsilon e^\rho \int_0^\infty A_\epsilon(s)\, e^{-se^\rho}ds = \frac{\pi}{2}. \tag{A.5}$$

The second integral may be integrated by parts so that

$$\int_0^\infty \frac{A_\epsilon(s)(1+2s)\sin(se^\rho)}{s}ds + \epsilon \int_0^\infty A'_\epsilon(s)\, e^{-se^\rho}ds = \frac{\pi}{2} - \epsilon A_\epsilon(0). \tag{A.6}$$

Using the result

$$e^{-se^\rho} = \frac{2}{\pi}\int_0^\infty \frac{t\sin(te^\rho)}{t^2+s^2}dt, \tag{A.7}$$

we may write

$$\int_0^\infty \frac{\sin(se^\rho)}{s}\left[A_\epsilon(s)(1+2s) + \frac{2\epsilon s^2}{\pi}\int_0^\infty \frac{A'_\epsilon(t)}{s^2+t^2}dt\right]ds$$

$$= \frac{\pi}{2} - \epsilon A_\epsilon(0). \tag{A.8}$$

Since

$$\int_0^\infty \frac{\sin(se^\rho)}{s}ds = \frac{\pi}{2}, \tag{A.9}$$

one possibility might be

$$A_\epsilon(s)(1+2s) + \frac{2\epsilon s^2}{\pi}\int_0^\infty \frac{A'_\epsilon(t)}{s^2+t^2}dt = 1 - \frac{2\epsilon}{\pi}A_\epsilon(0). \tag{A.10}$$

Making the substitution $t = s\tan\theta$ transform the above equation to

$$A_\epsilon(s)(1+2s) + \frac{2\epsilon s}{\pi}\int_0^{\frac{\pi}{2}} A'_\epsilon(s\tan\theta)\,d\theta = 1 - \frac{2\epsilon}{\pi}A_\epsilon(0). \tag{A.11}$$

The second integral may be integrated by parts to obtain

$$A_\epsilon(s)(1+2s) + \frac{2\epsilon}{\pi}\int_0^{\frac{\pi}{2}} A_\epsilon(s\tan\theta)\sin 2\theta d\theta = 1. \tag{A.12}$$

Thus we may find an expression for $A_\epsilon(0)$ by substituting $s = 0$ into the above equation, which yields

$$A_\epsilon(0) = \frac{\pi}{\pi + 2\epsilon}. \tag{A.13}$$

Taking the ordinary Laplace transform

$$F(p) = \int_0^\infty e^{-px} f(x)\,dx, \tag{A.14}$$

with inverse transformation

$$f(x) = \frac{1}{2\pi i}\int_{\epsilon-i\infty}^{\epsilon+i\infty} e^{px}F(p)\,ds, \tag{A.15}$$

of Eq. (A.5) with $x = e^{\rho}$ yields

$$\int_0^{\infty} A_{\epsilon}(s) \left[\frac{1+2s}{p^2+s^2} + \frac{\epsilon}{(p+s)^2} \right] ds = \frac{\pi}{2p}. \tag{A.16}$$

Making the substitution $s = p\tan\theta$ transforms the above equation to

$$\int_0^{\frac{\pi}{2}} A_{\epsilon}(p\tan\theta) \left[1 + 2p\tan\theta + \frac{\epsilon}{1+\sin 2\theta} \right] d\theta = \frac{\pi}{2}. \tag{A.17}$$

When $p = 0$ the above equation implies

$$A_{\epsilon}(0) = \frac{\pi}{\pi + 2\epsilon}, \tag{A.18}$$

as required. Since

$$\int_0^{\frac{\pi}{2}} d\theta = \frac{\pi}{2}, \tag{A.19}$$

then ideally we would like to have

$$A_{\epsilon}(p\tan\theta) \left[1 + 2p\tan\theta + \frac{\epsilon}{1+\sin 2\theta} \right] = 1, \tag{A.20}$$

from which it is apparent why the exact solution of Hocking [9] applies when $\epsilon = 0$. However, for ϵ nonzero the additional term is not a function of $p\tan\theta$ solely, and for this case we can only deduce an approximate analytical expression. Hence we assume

$$A_{\epsilon}(p\tan\theta) = \frac{1}{1 + 2p\tan\theta + a\epsilon}, \tag{A.21}$$

where a is a constant that may be determined from the requirement that

$$A_{\epsilon}(0) = \frac{\pi}{\pi + 2\epsilon}, \tag{A.22}$$

which implies $a = 2/\pi$. Some insight into why this provides such a good approximation might be inferred from calculating the difference

$$\begin{aligned} &\int_0^{\frac{\pi}{2}} A_{\epsilon}(p\tan\theta) \left[1 + 2p\tan\theta + \frac{\epsilon}{1+\sin 2\theta} \right] d\theta \\ &\quad - \int_0^{\frac{\pi}{2}} A_{\epsilon}(p\tan\theta) \left(1 + 2p\tan\theta + a\epsilon \right) d\theta, \end{aligned} \tag{A.23}$$

which is seen to be minimized since

$$\begin{aligned} \epsilon \int_0^{\frac{\pi}{2}} A_{\epsilon}(p\tan\theta) \left[\frac{1}{1+\sin 2\theta} - a \right] d\theta &\le \epsilon A_{\epsilon}(0) \int_0^{\frac{\pi}{2}} \left[\frac{1}{1+\sin 2\theta} - a \right] d\theta \\ &= \epsilon A_{\epsilon}(0) \left(1 - \frac{\pi a}{2} \right) \\ &= 0, \end{aligned} \tag{A.24}$$

for $a = 2/\pi$ (recall $A_\epsilon(s) \to 0$ as $s \to \infty$). Thus we have the approximate analytical expression

$$A_\epsilon(s) = \frac{1}{1 + \frac{2\epsilon}{\pi} + 2s}, \tag{A.25}$$

which implies

$$\begin{aligned} k_\epsilon(\rho) &= \frac{4e^\rho}{\pi} \int_0^\infty \frac{\sin(se^\rho)}{1 + \frac{2\epsilon}{\pi} + 2s} ds \\ &= \frac{2e^\rho}{\pi} \left\{ \mathrm{Ci}\left[\frac{(\pi + 2\epsilon) e^\rho}{2\pi}\right] \sin\left[\frac{(\pi + 2\epsilon) e^\rho}{2\pi}\right] \right. \\ &\qquad \left. -\mathrm{si}\left[\frac{(\pi + 2\epsilon) e^\rho}{2\pi}\right] \cos\left[\frac{(\pi + 2\epsilon) e^\rho}{2\pi}\right] \right\}. \end{aligned} \tag{A.26}$$

B. Appendix - Velocity comparisons

Although the main problem has been studied using the two-sided Laplace transform to simplify the numerical analysis, equally well it could also have been analyzed using the Mellin transform

$$\Psi(s, \theta) = \int_0^\infty r^{*s-1} \psi^*(r^*, \theta)\, dr^*, \tag{B.1}$$

with inverse transformation

$$\psi^*(r^*, \theta) = \frac{1}{2\pi i} \int_{\epsilon - i\infty}^{\epsilon + i\infty} r^{*-s} \Psi(s, \theta)\, ds, \tag{B.2}$$

where $r^* = r/\ell$ and $\psi(r, \theta) = Ur\psi^*(r^*, \theta)$. The form of $\Psi(s, \theta)$ is identical to that of Eq. (4.21) for $\tilde{\psi}(s, \theta)$, and the approximate analytical solutions of $k_a^*(r^*)$ and $k_b^*(r^*)$ are identical to that of Eqs. (5.16) and (5.17) for $k_a(\rho)$ and $k_b(\rho)$ with e^ρ replaced with r^*. Now $K_i(s)$ denotes the Mellin transform of $k_i^*(r^*)$. For $\theta_0 = \pi/2$ the function $\Psi(s, \theta)$ has the simple form

$$\Psi(s, \theta) = \frac{\sin\theta \sin\left[s\left(\theta - \frac{\pi}{2}\right)\right] K_1(s) - \cos\theta \sin(s\theta) K_2(s)}{2s \cos(\pi s/2)}. \tag{B.3}$$

Hence we have

$$\frac{\partial \Psi}{\partial \theta}\left(s, \frac{\pi}{4}\right) = -\frac{\sqrt{2}}{4}\left[\frac{\sin(\pi s/4)}{s\cos(\pi s/2)} - \frac{\cos(\pi s/4)}{\cos(\pi s/2)}\right] K_b(s). \tag{B.4}$$

where $K_b(s) = K_1(s) - K_2(s)$. It may be shown that the inverse Mellin transform of $\cos(\pi s/4) / \cos(\pi s/2)$ is given by

$$\frac{\sqrt{2} r^* \left(r^{*2} + 1\right)}{\pi \left(r^{*4} + 1\right)}. \tag{B.5}$$

Similarly it may be shown that the inverse Mellin transform of $\sin(\pi s/4)/\cos(\pi s/2)$ is given by

$$\frac{\sqrt{2}r^*\left(r^{*2}-1\right)}{\pi\left(r^{*4}+1\right)}. \tag{B.6}$$

The inverse Mellin transform of $1/s$ is 1 for $0 < r^* < 1$ and 0 for $1 < r^* < \infty$. Hence by the convolution theorem for the Mellin transform, the inverse of $\sin(\pi s/4)/s\cos(\pi s/2)$ is given by

$$\frac{\sqrt{2}}{\pi}\int_0^1 \frac{r^*\left(r^{*2}-u^2\right)}{r^{*4}+u^4}du = \frac{1}{2\pi}\ln\left(\frac{r^{*2}+\sqrt{2}r^*+1}{r^{*2}-\sqrt{2}r^*+1}\right). \tag{B.7}$$

By applying the convolution theorem for the Mellin transform again to $\partial\Psi/\partial\theta\,(s,\pi/4)$ we have

$$\begin{aligned}\frac{\partial\psi^*}{\partial\theta}\left(r^*,\frac{\pi}{4}\right) = -\frac{\sqrt{2}}{4\pi^2}\int_0^\infty \frac{r^*}{u^2}\left[\ln\left(\frac{u^2+\sqrt{2}u+1}{u^2-\sqrt{2}u+1}\right)-\frac{2\sqrt{2}u\left(u^2+1\right)}{u^4+1}\right]\\ \times\left\{\mathrm{Ci}\left[\frac{(\pi-2)\,r^*}{2\pi u}\right]\sin\left[\frac{(\pi-2)\,r^*}{2\pi u}\right]-\right.\\ \left.\mathrm{si}\left[\frac{(\pi-2)\,r^*}{2\pi u}\right]\cos\left[\frac{(\pi-2)\,r^*}{2\pi u}\right]\right\}du,\end{aligned} \tag{B.8}$$

which may be evaluated numerically using standard routines and we have assumed the approximate analytical expression Eq. (5.17) for $k_b^*(r^*)$ obtained by replacing e^ρ with r^*.

C. Appendix - Nomenclature

$\psi(r,\theta)$	stream function in physical variables (r,θ).
$\bar{\psi}(\rho,\theta)$	$(Ur)^{-1}\psi(r,\theta)$; modified stream function in variables (ρ,θ) where $\rho=\ln(r/\ell)$.
$\tilde{\bar{\psi}}(s,\theta)$	two-sided Laplace transform of $\bar{\psi}(\rho,\theta)$.
$\psi^*(r^*,\theta)$	$(Ur)^{-1}\psi(r,\theta)$; modified stream function in variables (r^*,θ) where $r^*=r/\ell$.
$\Psi(s,\theta)$	Mellin transform of $\psi^*(r^*,\theta)$.
$k_1(\rho)$, $k_2(\rho)$	$\partial^2\bar{\psi}/\partial\theta^2(\rho,0)\equiv rT_{r\theta}\vert_{\theta=0}/\mu U$, $\partial^2\bar{\psi}/\partial\theta^2(\rho,\theta_0)\equiv rT_{r\theta}\vert_{\theta=\theta_0}/\mu U$.
$\hat{k_1}$, $\hat{k_2}$	$k_1(\infty)$, $k_2(\infty)$.
$\tilde{k}_1(\rho)$, $\tilde{k}_2(\rho)$	two-sided Laplace transform of $k_1(\rho)$, $k_2(\rho)$.
$k_a(\rho)$, $k_b(\rho)$	$k_1(\rho)+k_2(\rho)$, $k_1(\rho)-k_2(\rho)$.
$\hat{k_a}$, $\hat{k_b}$	$\hat{k_1}+\hat{k_2}$, $\hat{k_1}-\hat{k_2}$.
$\tilde{k}_a(\rho)$, $\tilde{k}_b(\rho)$	$\tilde{k}_1(\rho)+\tilde{k}_2(\rho)$, $\tilde{k}_1(\rho)-\tilde{k}_2(\rho)$.
$k_1^*(r^*)$, $k_2^*(r^*)$	$\partial^2\psi^*/\partial\theta^2(r^*,0)\equiv rT_{r\theta}\vert_{\theta=0}/\mu U$,

	$\partial^2\psi^*/\partial\theta^2\,(r^*,\theta_0) \equiv rT_{r\theta}|_{\theta=\theta_0}/\mu U$.
$k_a^*\,(r^*)$, $k_b^*\,(r^*)$	$k_1^*\,(r^*)+k_2^*\,(r^*)$, $k_1^*\,(r^*)-k_2^*\,(r^*)$.
$K_1\,(s)$, $K_2\,(s)$	Mellin transform of $k_1^*\,(r^*)$, $k_2^*\,(r^*)$.
$K_a\,(s)$, $K_b\,(s)$	$K_1\,(s)+K_2\,(s)$, $K_1\,(s)-K_2\,(s)$.
ℓ_1, ℓ_2	slip lengths along $\theta=0$ and $\theta=\theta_0$.
$\tilde{\ell}$	ℓ_1/ℓ_2.
ℓ	slip length for that case $\ell_1=\ell_2=\ell$.
$P\,(\rho)$, $Q\,(\rho)$	functions defined by the inverse transforms Eq. (4.25) and given explicitly by Eq. (5.2) for $\theta_0=\pi/2$.

Miccal T. Matthews and James M. Hill
University of Wollongong
School of Mathematics and Applied Statistics
Wollongong, N.S.W. 2522
Australia
e-mail miccal@uow.edu.au

(Received: November 9, 2005)

Published Online First: June 8, 2006